JACS
JOURNAL OF THE AMERICAN CHEMICAL SOCIETY

COMMUNICATION

pubs.acs.org/JACS

Macroscopic Wall Number Analysis of Single-Walled, Double-Walled, and Few-Walled Carbon Nanotubes by X-ray Diffraction

Don N. Futaba,*[,†] Takeo Yamada,[†] Kazufumi Kobashi,[†] Motoo Yumura,[†] and Kenji Hata[†,‡]

[†]Nanotube Research Center, National Institute of Advanced Industrial Science and Technology (AIST), Tsukuba 305-8565, Japan
[‡]Japan Science and Technology Agency (JST), Kawaguchi 332-0012, Japan

Supporting Information

ABSTRACT: The layer number is of great importance for nanocarbon materials, such as carbon nanotubes (CNTs) and graphene. While simple optical methods exist to evaluate few-layer graphene, equivalent analysis for CNTs is limited to transmission electron microscopy. We present a simple macroscopic method based on the (002) X-ray diffraction peak to evaluate the average wall number of CNTs in the range from single- to few-walled. The key was the finding that the (002) peak could be decomposed into two basic components: the intertube structure (outer-wall contacts) and the intratube structure (concentric shells). Decomposition of the peaks revealed a linear relationship between the average wall number and the ratio of the intertube and intratube contributions to the (002) peak. Good agreement with CNTs having average wall numbers ranging from 1 to ∼5 demonstrated this as a macroscopic method for average wall number analysis.

For nanocarbon materials, as represented by carbon nanotubes (CNTs) and graphene, the number of layers (graphene shells or layers) is a fundamental structural parameter on which many physical and chemical properties depend. This is particularly true for nanocarbon materials composed of few (∼5) layers because this region is far from the three-dimensional (3D) bulk limit (i.e., nanofibers or bulk graphite). As such, on the basis of the number of layers, CNTs are specifically categorized as single-walled CNTs (SWCNTs), double-walled CNTs (DWCNTs), and multiwalled CNTs (MWCNTs). Similarly, graphene is defined as a single layer of graphite. Several examples are provided to exemplify the large differences between these nanocarbon materials. SWCNTs consist of only a single graphene shell and therefore can be exceptionally thin (∼1 nm). Furthermore, the electronic character can be semiconducting depending on their chirality[1] and possess an exceptionally high specific surface area[2] that is useful for various applications from supercapacitors[3] to highly conductive CNT materials.[4] DWCNTs possess several advantages over SWCNTs, including their higher mechanical strength and increased chemical and thermal stabilities. Their high current stability makes them favored for field-emission applications,[5] and the double-walled structure allows for selective functionalization of the outer wall.[6] On the other hand, unlike SWCNTs and DWCNTs, MWCNTs possess similar electrical (metallic), mechanical, chemical, and thermal stabilities resulting from the weak coupling between cylinders. Combined with their low cost, MWCNTs have been the most promising candidates for industrial applications because of the homogeneous properties among individual MWCNTs in an ensemble. An apt illustration of this advantage is MWCNT-based LSI vias.[7] Similarly, the properties of graphene also vary with layer number. While single-layer graphene is a zero-gap semiconductor,[8] the conduction and valence bands begin to overlap with increasing layer number and beyond ∼10 layers approach the 3D limit of graphite.[9]

Therefore, identifying the average wall number of CNTs is paramount in understanding their properties and directing them toward the appropriate applications. Consequently, numerous efforts have been carried out to develop methods to characterize the number of graphene layers in nanocarbon materials. First, for few-layer graphene, even an optical microscope can be useful to discriminate the number of layers.[10] More quantitatively, Raman spectroscopy can be used as an indicator of layer number from the relative peak intensities of the disorder peak double resonance (G′) at ∼2710 cm^{-1} and the graphitic peak (G) at ∼1380 cm^{-1} (i.e., the G′/G ratio) because the G′ intensity increases with decreasing layer number.[11] This allows for an unambiguous, high-throughput estimation of the layer number on a macroscopic scale. In contrast, for CNTs, such straightforward spectroscopic methods have not been demonstrated. Raman spectroscopy has been reported to identify the radial breathing modes (RBMs) of MWCNTs. However, because the RBMs could only be detected from the innermost shells, this method could not be generalized to estimate the layer number.[12] Therefore, people still rely on the direct observation by transmission electron microscopy (TEM) to characterize the average wall number. In this method, high-resolution microscopic images of dispersed CNTs are taken and manually inspected for the wall number to create a histogram.[13] This process is not only microscopic but also time-consuming.

X-ray diffraction (XRD) is a well-established and powerful macroscopic structural characterization tool that has been applied to measure the "*d* spacing" between graphene layers. For example, the MWCNT interlayer spacing has been measured by the location of the (002) peak.[14] The SWCNT intertube packing (lattice constant) has been characterized by the location of the (10) peak.[15] Furthermore, the SWCNT diameter distribution[16] has been characterized by detailed analysis of the (10) peak.[17]

Received: January 20, 2011
Published: March 28, 2011

ACS Publications © 2011 American Chemical Society

dx.doi.org/10.1021/ja2005994 | *J. Am. Chem. Soc.* 2011, 133, 5716–5719

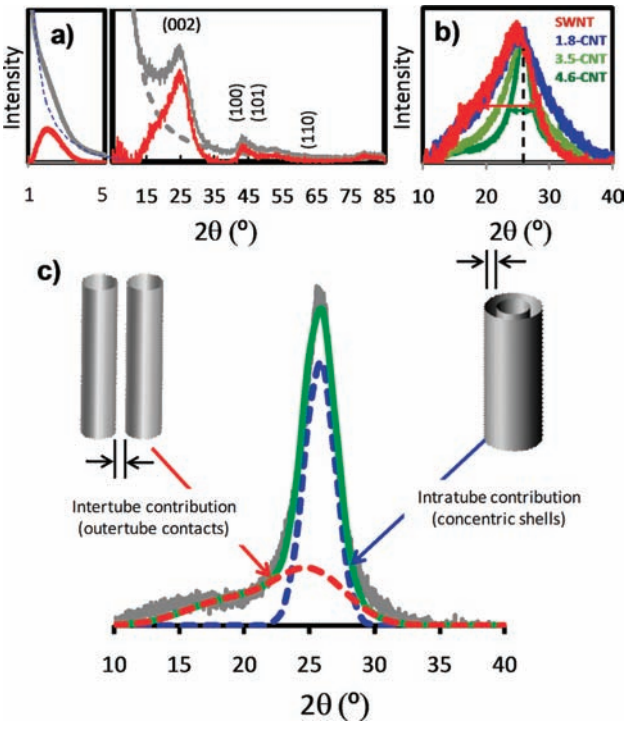

Figure 1. XRD of carbon nanotubes. (a) XRD $\theta-2\theta$ mosaic of an SWCNT sample (gray, raw data; red, after background subtraction). (b) (002) XRD peak for CNTs of increasing average wall number (1−4.6). (c) Conceptual illustration of the decomposition of the total (002) peak (green) into the two basic contributions: (red) intertube structure (outer-wall contacts) and (blue) intratube structure (concentric shells).

In this work, we focused on the XRD (002) peak and developed a simple macroscopic method to determine the average wall number of CNTs ranging from SWCNTs to few-walled MWCNTs. The key was the finding that the (002) peak could be decomposed into two basic components: the intertube structure (outer-wall contacts) and the intratube structure (concentric shells). Average wall number estimation became possible because the contribution of the intratube structure to the (002) peak increased linearly with wall number while the contribution of the intertube structure did not.

We start by introducing a typical XRD pattern of SWCNTs (Figure 1a) to identify the fundamental peaks and explain why we focused on the (002) peak. The XRD pattern shows a series of peaks that could be categorized into two types. Peaks at high angles reflect structure from an individual CNT, whereas peaks at low angles reflect structure resulting from an ensemble of CNTs. Specifically, the (110), (101), and (100) peaks observed at higher angles (above ∼40°) reflect the atomic structure of the graphene sheet, and the peak at lower angles (<5°) reflects the intertube packing. The (002) peak, which lies between these two regions, is unique because it can have contributions from both an individual tube and the ensemble.

To address this issue, we studied the (002) peak profile over a wide range of CNT samples. Commercially available HiPco and CoMoCAT SWCNTs and Nanocyl (∼5 walls) and Nikkiso (>30 walls) MWCNTs were characterized. In addition, we synthesized a family of CNT samples differing only by average wall number. Specifically, CNTs with average wall number varying from 1 to ∼5 by engineering the catalyst thin film[13,18] were synthesized by water-assisted chemical vapor deposition.[19] The average wall numbers were directly characterized by TEM. As a result, our samples included nearly 100% SWCNTs and 1.2, 1.8, 3.5, and 4.6-walled CNTs. The as-grown CNT forests were made into solid sheets[3] to increase the signal intensity by increasing the material density by ∼20-fold (density ≈ 0.5 g/cm^3). This processing induced no change in the (002) peak profile. Standard $\theta-2\theta$ XRD was carried out on this family of samples using a Rigaku X-ray diffractometer with a Cu Kα X-ray source at a total power of 1.2 kW, and the (002) peaks were analyzed.

As shown in Figure 1b, the (002) peak of a SWCNT forest (red line) exhibited a profile both fairly broad and complex. The (002) peak for CNTs originates from the c axis interlayer spacing, as in graphite. However, it should be noted that in principle, SWCNTs do not possess an intratube structure, so an individual SWCNT would not be expected to exhibit a (002) peak. This means that the (002) peak for SWCNTs originates entirely from contacts between the outer shells of adjacent SWCNTs (outer-wall contacts). Because the intertube contribution consists of an asymmetric distribution of d spacings as small as the graphitic limit (∼0.34 nm) and larger, it follows that the resultant (002) peak should also be asymmetric and broad. Further broadening is also expected to occur because of curvature effects due to the cylindrical shape.

In contrast, the (002) peaks of DWCNTs (blue line) and few-walled MWCNTs (green lines) increased in both sharpness and symmetry with increasing average wall number in comparison with the broad, asymmetric (002) peak from SWCNTs (Figure 1b). This is because the intratube (concentric shell) structure of MWCNTs contributes to the (002) peak.[20] As the concentric shells are nearly uniformly graphitically spaced (∼0.34 nm), the corresponding (002) peak is expected to be sharp and symmetric. These results demonstrate that the (002) peak is composed of two basic components, one reflecting the intertube structure (outer-wall contacts) and the other representing the intratube structure (concentric walls).

Motivated by these results, we developed a model to analytically decompose the (002) peak into the two basic components. To first order, we assumed that the (002) profile could be completely described by the superposition of the asymmetric intertube and symmetric intratube structures (Figure 1c, inset). Here, the outer-wall contacts describe the intertube structure while the concentric shells describe intratube structure. Therefore, the (002) profile could be described as $I_{002}(2\theta) = A \cdot I_{inter}(2\theta) + B \cdot I_{intra}(2\theta)$, where I_{002}, I_{inter}, and I_{intra} are the intensities as a function of diffraction angle (2θ) for the total (002) peak, the intertube structure, and the intratube structure, respectively, and A and B are the relative contributions of I_{inter} and I_{intra}, respectively, to I_{002} (Figure 1c).

First, the intertube contribution (I_{inter}) was estimated as the empirically measured (002) profile of SWCNTs because the interlayer structure is solely derived from its intertube structure (i.e., there are no concentric shells) (Figure 2a, red line). This contribution was mathematically described as the sum of two Gaussians (Figure 2a, gray lines). Second, the intratube contribution (I_{intra}) was approximated by a Gaussian as $I_{intra}(2\theta) = \exp[-(2\theta - P)^2/2C^2]$, where P is the central peak position, C^2 is the variance, and 2θ is the diffraction angle. Both P and C^2 were treated as adjustable fitting parameters because the position (i.e., the interlayer spacing of MWCNTs) and broadness of the (002) peak have been reported to increase with diameter and layer number.[14,20]

With these analytical descriptions of the intertube and intratube contributions, we fitted this model to the normalized (002) peak for

dx.doi.org/10.1021/ja2005994 |J. Am. Chem. Soc. 2011, 133, 5716–5719

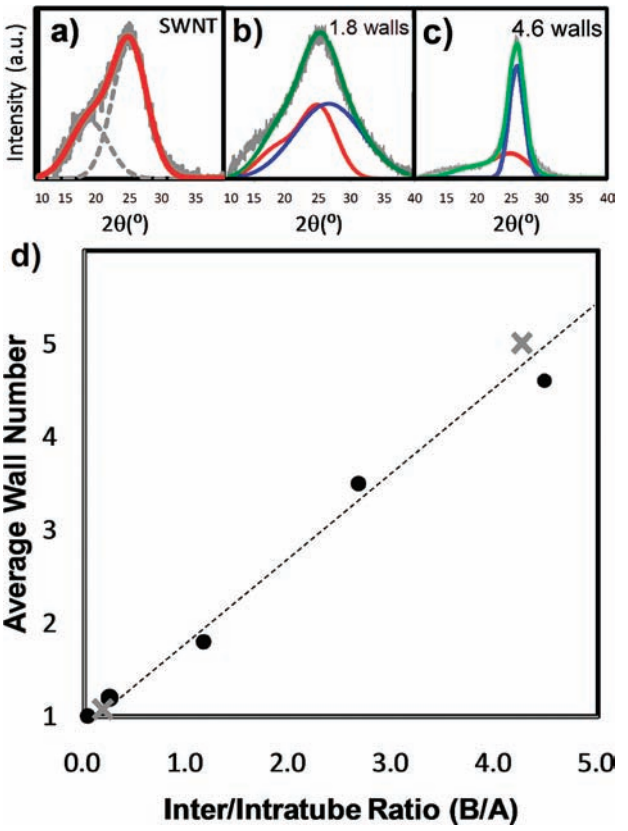

Figure 2. Relationship between average wall number and intertube/intratube ratio. (a−c) Demonstration of the decomposition of the (002) peaks for samples with average wall numbers from 1 to 4.6. (intertube contribution, red line; intratube structure, blue line; sum of intertube and intratube contributions, green line; experimental data, gray line). (d) Linear relationship between the known average wall number determined by TEM and the intertube/intratube ratio (B/A) from the decomposition fitting (●, aligned samples; ×, randomly oriented samples).

a MWCNT sample having ∼4.6 walls. The fitting algorithm converged with a standard error of 0.0256 and a correlation coefficient of 0.9945, indicating a good fit to this model. The generated fitting parameters provided a quantitative description of the (002) peak in terms of the Gaussian peak position P and variance C^2 and the relative intratube and intertube contributions A and B (Figure 1c).

We fit this model to the experimentally obtained (002) peaks for the family of five CNT samples differing in average wall number. The results for three of the samples are shown in Figure 2, where the individual intertube and intratube contributions are overlaid on the experimental data (Figure 2). The good agreement demonstrated that the model was adaptable to CNTs ranging from SWCNTs to few-walled MWCNTs. [It should be noted that our model could not be applied to thick MWCNTs with tens of layers, as a similar analysis on Nikkiso MWCNTs (>30 walls) failed to converge.] We can glean several important points from the resulting data (Figure 2). First, the contribution of the intertube structure, A, as indicated by the relative heights of the red profile, decreased with increasing wall number. Second, the intratube (i.e., concentric walls) contribution, B, as indicated by the height of the Gaussian peak (Figure 2b,c, blue) increased. Third, the width (variance, C^2) of the intratube contribution decreased with increasing average wall number. These trends

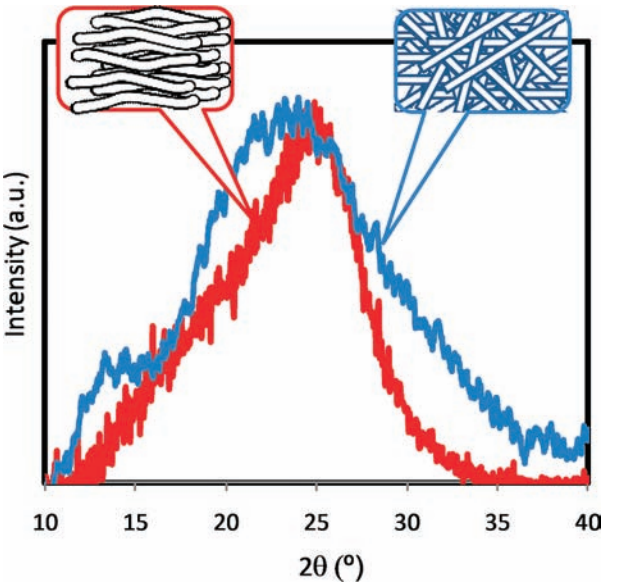

Figure 3. Difference in (002) peak profiles of aligned (red) and randomly oriented (HiPco) samples (blue).

indicate that the dominant contribution to the (002) peak progressively shifted from the intertube structure (i.e., outer-wall contacts) for SWCNTs to the intratube structure (concentric shells) with increasing average wall number.

Significantly, when we plotted the average wall number versus the ratio of the intratube and intertube contributions to the (002) peaks (i.e., $\rho \equiv B/A$), we found a linear relationship between the two. Specifically, for the fitted (002) profiles discussed above, we calculated the values of ρ and then plotted the average wall number ($N_{w,av}$) versus ρ, which revealed a linear relationship (Figure 2d, black dots). Fitting this data to a linear function yielded the quantitative expression $N_{w,av} = 0.862\rho + 1$. This observation constitutes our central experimental finding, and it is important because this linear relationship could be used to construct a macroscopic method for evaluating the average wall number of CNTs by XRD (see the Supporting Information). The average wall number for a macroscopic sample consisting of SWCNTs to few-walled MWCNTs could be estimated by measuring the B/A ratio from the (002) peak.

It is important to note that while the shape of the intratube contribution is common for all of the macroscopic aggregations of CNTs, the intertube contribution changes depending on the aggregate form. In this regard, two basic forms would exist: aligned and randomly oriented CNTs. In the case of aligned CNTs, the outer-tube contacts between individual tubes extend over long spans at nearly graphitic spacing as a result of the high order. In contrast, for randomly oriented samples, the outer-tube contacts between individual tubes could be very short. Therefore, the distribution of d spacings should be relatively sharp for aligned samples but broader for random samples. To address this point, we applied our model to randomly aligned samples: HiPco and CoMoCAT[22] SWCNTs and Nanocyl (∼5 walls) MWCNTs. Measurement of the randomly oriented SWCNTs showed a (002) peak that differed from the one for the aligned samples, with a peak shift to a lower 2θ angle (larger d spacing) and a pronounced peak at ∼15° (Figure 3). Using the HiPco (002) peak as the intertube contribution for the model, the peaks for the CoMoCAT SWCNTs and Nanocyl MWCNTs were each

dx.doi.org/10.1021/ja2005994 |J. Am. Chem. Soc. 2011, 133, 5716–5719

fitted to this "random" model, and the results are plotted as the × symbols in Figure 2d. Estimation of the average wall numbers on the basis of the B/A ratios (1.1 and 4.7) agreed well with the average wall numbers (1 and ~5) observed by TEM for CoMoCAT SWCNTs and Nanocyl MWCNTs, respectively (Figure 2d). This result demonstrates the generality of our approach for estimating the average wall numbers of CNTs of various forms.

In summary, we have developed a simple macroscopic method for determining the average wall number of CNTs in the range from SWCNTs to few-walled MWCNTs using the (002) XRD peak. This method provides a fast and easy macroscopic wall number assessment of CNTs to compliment TEM. In contrast to TEM, our approach based on XRD can provide an accurate estimation of the average wall number for a macroscopic sample in a short time period. The method is dependent on the form of the CNTs and currently limited to few-walled CNTs because the (002) peak becomes exceptionally sharp for MWCNTs with tens of shells. Use of a Lorentzian rather than a Gaussian may be more appropriate to characterize these CNTs[21] and might enable our approach to be extended further.

■ ASSOCIATED CONTENT

Supporting Information. Direct comparison of average wall number analyses by TEM and XRD. This material is available free of charge via the Internet at http://pubs.acs.org.

■ AUTHOR INFORMATION

Corresponding Author
d-futaba@aist.go.jp

■ ACKNOWLEDGMENT

We acknowledge support from the Nanotechnology Program "Carbon Nanotube Capacitor Development Project" (2006-2011) by the New Energy and Industrial Technology Development Organization (NEDO).

■ REFERENCES

(1) Saito, R.; Fujita, M.; Dresselhaus, G.; Dresselhaus, M. S. *Appl. Phys. Lett.* **1992**, *60*, 2204.
(2) Peigney, A.; Laurent, C.; Flahaut, E.; Bacsa, R. R.; Rousset, A. *Carbon* **2001**, *39*, 507.
(3) Futaba, D. N.; Hata, K.; Yamada, T.; Hiraoka, T.; Hayamizu, Y.; Kakudate, Y.; Tanaike, O.; Hatori, H.; Yumura, M.; Iijima, S. *Nat. Mater.* **2006**, *5*, 987.
(4) Sekitani, T.; Nakajima, H.; Maeda, H.; Fukushima, T.; Aida, T.; Hata, K.; Someya, T. *Nat. Mater.* **2009**, *8*, 494.
(5) Seko, K.; Kinoshita, J.; Saito, Y. *Jpn. J. Appl. Phys.* **2005**, *44*, L743.
(6) Muramatsu, M.; Kim, Y. A.; Hayashi, T.; Endo, M.; Yonemoto, A.; Arikai, H.; Okino, F.; Touhara, H. *Chem. Commun.* **2005**, 2002.
(7) Nihei, M.; Kawabata, A.; Kondo, D.; Horibe, M.; Sato, S.; Awano, Y. *Jpn. J. Appl. Phys.* **2005**, *44*, 1626.
(8) Novoselov, K. S.; Geim, A. K.; Morozov, S. V.; Jiang, D.; Zhang, Y.; Dubonos, S. V.; Grigorieva, I. V.; Firsov, A. A. *Science* **2004**, *306*, 666.
(9) Partoens, B.; Peeters, F. M. *Phys. Rev. B* **2006**, *74*, No. 075404.
(10) Casiraghi, C.; Hartschuh, A.; Lidorikis, E.; Qian, H.; Harutyunyan, H.; Gokus, T. *Nano Lett* **2007**, *7*, 2711.
(11) Ferrari, A. C.; Meyer, J. C.; Scardaci, V.; Casiraghi, C.; Lazzeri, M.; Mauri, F.; Piscanec, S.; Jiang, D.; Novoselov, K. S.; Roth, S.; Geim, A. K. *Phys. Rev. Lett.* **2006**, *97*, No. 187401.
(12) Zhao, X.; Ando, Y.; Qin, L.-C.; Kataura, H.; Maniwa, Y.; Saito, R. *Chem. Phys. Lett.* **2002**, *361*, 169.
(13) Yamada, T.; Namai, T.; Hata, K.; Futaba, D. N.; Mizuno, K.; Fan, J.; Yudasaka, M.; Yumura, M.; Iijima, S. *Nat. Nanotechnol.* **2006**, *1*, 131.
(14) Saito, Y.; Yoshikawa, T.; Bandow, S.; Tomita, M.; Hayashi, T. *Phys. Rev. B* **1993**, *48*, 1907.
(15) Thess, A.; Lee, R.; Nikolaev, P.; Dai, H.; Petit, P.; Robert, J.; Xu, C.; Lee, Y. H.; Kim, S. G.; Rinzler, A. G.; Colbert, D. T.; Scuseria, G. E.; Tománek, D.; Fischer, J. E.; Smalley, R. E. *Science* **1996**, *273*, 483.
(16) Wang, B. N.; Bennett, R. D.; Verploegen, E.; Hart, A. J.; Cohen, R. E. *J. Phys. Chem. C* **2007**, *111*, 5859.
(17) Abe, M.; Kataura, H.; Kira, H.; Kodama, T.; Suzuki, S.; Achiba, Y.; Kato, K.-i.; Takata, M.; Fujiwara, A.; Matsuda, K.; Maniwa, Y. *Phys. Rev. B* **2003**, *68*, No. 041405.
(18) Zhao, B.; Futaba, D. N.; Yasuda, S.; Akoshima, M.; Yamada, T; Hata, K. *ACS Nano* **2009**, *3*, 108.
(19) Hata, K.; Futaba, D. N.; Mizuno, K.; Namai, T.; Yumura, M.; Iijima, S. *Science* **2004**, *306*, 1362.
(20) Reznik, D.; Olk, C.; Neumann, A.; Copley, J. *Phys. Rev. B* **1995**, *52*, 116.
(21) Gommes, C.; Blacher, S.; Dupont-Pavlovsky, N.; Bossuot, C.; Marguillier, D.; Fonseca, A.; Nagy, J. B.; Pirard, J.-P. *Colloids Surf., A* **2004**, *241*, 155.
(22) Resasco, D. E.; Alvarez, W. E.; Pompeo, F.; Balzano, L.; Herrera, J. E.; Kitiyanan, B.; Borgna, A. *J. Nanopart. Res.* **2002**, *4*, 131.